Multi-loop Damping and Tracking Strategy Emulating a Butterworth Pattern for Accurate Nanopositioning

Mohammed Altaher[1] and Sumeet S. Aphale[2]

[1] University of Aberdeen, Aberdeen, United Kingdom, <mohammed.altaher@abdn.ac.uk>
[2] University of Aberdeen, Aberdeen, United Kingdom, <s.aphale@abdn.ac.uk>

Abstract. Control schemes for nanopositioners typically combine damping and tracking. Due to the positioning performance requirements of the nanopositioning system, it is desirable for the closed-loop frequency response of the nanopositioner to mimic ripple-free pass-band low-pass characteristics. Earlier reports are available on simultaneous damping and tracking control emulating a Butterworth filter design, but this technique only incorporates a single integrator for tracking, which is inadequate for error-free tracking of the triangular and ramp-like signals typically used as input to nanopositioning systems. Double integral tracking guarantees error-free tracking, but is difficult to implement due to phase-related stability issues. In this work, a dual-loop integral tracking algorithm is proposed. Using simulation, it is shown that in the presence of hysteresis, the proposed dual-loop scheme delivers a more accurate positioning performance than the traditional single-loop integral tracking strategy.

Keywords: Butterworth pattern, Nanopositioner, Damping, Tracking.

1 Introduction

A nanopositioner is a mechatronic system designed to deliver precise positioning with nano scale accuracy. In precise position control, there are many desired control objectives that aim to obtain a fast response with no overshoot and accurate set-point tracking, a very high travel range and a high bandwidth. All of these objectives can be improved by using a feedback controller; however, the complexity of the controller varies depending on which control objective is most important [6].

For systems that undergo parameter changes, such as a change in damping and resonance frequency due to loading, control designs offering good gain and phase margins are most suited. Nanopositioning systems exhibit various types of uncertainty due to a change in sample mass, mechanical ageing, sensors and actuator drifts. Furthermore, many control schemes have a tendency to exacerbate the high frequency out-of-bandwidth unmodelled dynamics [13]. In order to overcome these issues, control schemes have been employed to improve the performance of nanopositioners, which must be robust under the presence of parameter uncertainties. In addition to resonance and parameter uncertainty, nanopositioners are also marred by nonlinear effects such as hysteresis and creep due to the piezoelectric actuators that are popularly employed in these systems. Therefore, along with robust damping controllers and high gain, high-bandwidth tracking control is an essential component of the overall control scheme.

For quite some time, damping and tracking controllers have been designed sequentially (damping first, tracking later) and implemented in an inner-outer loop fashion. It has been shown that the sequential design is sub-optimal in terms of obtainable positioning performance and simultaneous damping and therefore tracking control design has been proposed [8]. Using the Butterworth filter, which has the desirable properties of a flat, ripple-free passband and a quick roll-off at high frequencies as a motivation, simultaneous damping and tracking schemes that emulate a Butterworth filter have been proposed in [9].

In nanopositioning applications, the typical scanning pattern is a raster, generated by employing a slow ramp along one axis and a fast triangle wave along the other. Both the input signals therefore have non-zero velocity and it is impossible to track them error-free with a single integral tracking control. This paper provides a strategy to simultaneously design the damping and the multi-loop tracking controllers in order to mimic the Butterworth filter pattern. Simulations are presented to support the proposed theory.

The paper is organised as follows: section II presents the linear model for axes on the nanopositioning platform, as well as the nonlinear Bouc-Wen model for the hysteresis exhibited by the actuator on this axis. The Butterworth filter pattern for the proposed multi-loop control strategy is presented in section III. Simulated open- and closed-loop, time-domain and frequency-domain results are given in Section IV, where the theoretical error analysis for the proposed control scheme is also presented. Robustness of the control scheme in the presence of resonance frequency shift is also examined in this section. Section V concludes the paper.

2   System Modelling

The dynamics of the nano axis has linear and nonlinear components; thus, the axis is modelled as a linear second-order transfer function and a Bouc Wen model for hysteresis.

2.1   Linear Dynamics Model

The mechanical system of the nanopositioning platform is shown in Fig. 1 (a) [1], which can be characterised and simplified by a spring-damper system, as shown in Fig. 1 (b) [10]. The axis of the nanopositioning platform is equipped with a capacitive sensor for position measurement. The equation of motion for this system is given by:

$$M_p\ddot{d} + c_f\dot{d} + (K_a + k_f)d = F_a \tag{1}$$

The system dynamics is regulated by the piezoelectric actuator force that moves the nanopositioning stage. The movement of the piezo actuators is manifested by expansion and contraction in response to an input voltage stimulus. Thus, (F_s) is the measured force acting between the actuator and the mass of the platform (M_p) in the vertical direction. The stiffness of the actuator is denoted by (K_a) and the force by (F_a). A force

sensor is collocated with the actuator and measures the load force F_s. Equation 1 can now be rewritten as follows:

$$M_p \ddot{d} + c_f \dot{d} + k = F_a \tag{2}$$

The relationship between the applied force (F_a) and the displacement d is described as
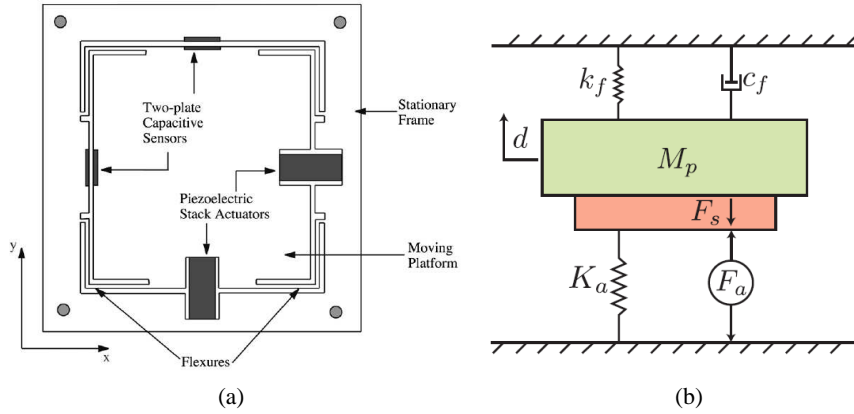

(a) (b)

Fig. 1. a- A simple schematic of a piezo-stack actuated two-axis nanopositioner; b- The equivalent mass-spring-damper model for one axis of the nanopositioner

in the following transfer function:

$$G_{dF_a}(s) = \frac{d}{F_a} = \frac{1}{M_p s^2 + c_f s + k} \tag{3}$$

This can be described in the frequency domain as a second-order system and the transfer function can be written in the form (4):

$$G(s) = \frac{\sigma^2}{s^2 + 2\zeta\omega_p s + \omega_p^2} , \tag{4}$$

where ζ is the damping ratio, ω_p is the natural frequency and σ^2 is the DC gain of the platform. The investigated system is represented by the linear dynamics transfer function below; this is characterised by its first resonant mode and given by:

$$G(s) = \frac{4.746 * 10^8}{s^2 + 910.1s + 2.927 * 10^8} , \tag{5}$$

where the value of the damping ratio (ζ) is 0.0266 and the natural frequency $f_n = 2\pi * \omega_p$, where the value of the ω_p^2 is $2.927 * 10^8$ and σ^2 is $4.746 * 10^8$.

Figure 2 shows that the modelled-based frequency response and the measurement-based, which have been superimposed, are almost identical.
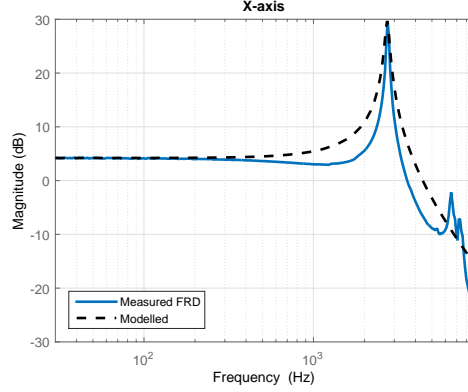

Fig. 2. Comparison between the measured- and model-based magnitude response for the x-axis of the system in. The slight mismatch in the width of the resonant mode is due to the sensor and amplifier dynamics, along with the nanopositioner axis dynamics included in the measured response

2.2 Hysteresis Model

Nonlinear effects are usually unmodelled and tracking is enforced to minimise the effect of nonlinearities on the actual trace. Hysteresis is a dynamic characteristic present in many physical systems such as piezo actuators. Hysteresis in piezo actuators can lead to problems such as an increase in undesirable inaccuracy or oscillation and instability [14]. Therefore, any control strategy must be designed to accommodate uncertain time-varying nonlinear systems.

The hysteresis in this work has been described by the Bouc Wen model [3, 11, 12]. The Bouc Wen describes the equation of motion for the nanopositioning platform using its nonlinear differential equations, as in equation (6):

$$\begin{cases} m\ddot{x} + b\dot{x} + kx = k(du - h) \\ \dot{h} = \alpha d\dot{u} - \beta |\dot{u}| h - \gamma \dot{u} |h| \end{cases} \tag{6}$$

where h represents the nonlinear relation between the lag force (applied voltage) u and the displacement x. The coefficients m, b, k and d denote the effective mass, damping coefficient, mechanical stiffness and effective piezoelectric coefficients respectively. It is noted that hysteresis for the proposed system is rate-independent, hence Bouc Wen has been selected as opposed to other models because it is rate-independent and simple. Its parameters, α, β, d and γ, have been realised in MATLAB Simulink and determined so the hysteresis loop produced by Bouc Wen can accurately match the experimental data on the nanopositioning platform. The parameters of Bouc Wen are selected as follows in (7):

$$\left\{ \alpha = 0.26, \beta = 0.005, \gamma = 0.00068, \text{d=2 } \mu\text{m per volt} \right\} \tag{7}$$

The proposed hysteresis model is investigated by applying a 50 volt peak amplitude sinusoidal signal of 10 Hz to the platform and the hysteresis cycle is thereby generated. Figure 3 illustrates the generated hysteresis in the open-loop, which is associated with a single axis of the nanopositioning platform. In Fig. 3, a comparison can be seen
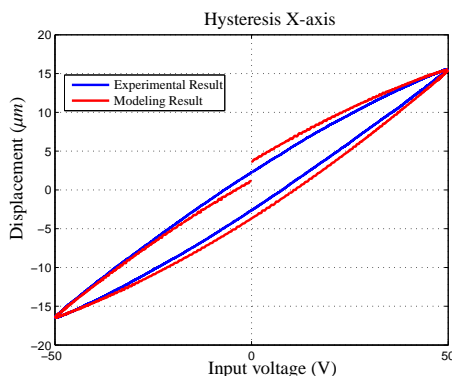

Fig. 3. Measured and modelled hysteresis loops show that the hysteresis model accurately captures the hysteresis of the piezo actuator

between the experimental and the modelling result, where the x-axis represents the input voltage and the y axis is the generated displacement. It can be seen from Fig. 3 that the open-loop exhibits strong nonlinearity. A system exhibiting such hysteresis is severely limited in its performance. The hysteresis loop provides a rate-independent relationship between the applied voltage and the generated displacement.

3 Control Strategy

Nanopositioning systems are lightly damped and highly likely to exhibit mechanical resonance when there is any sudden change in the voltage applied to the platform. Thus, the use of damping controllers is necessary, the damping to damp resonance and the tracking controllers to treat nonlinearity. Consequently, minimising the error is considered the most important control object in the nanopositioning application. This section will explain the traditional approach and the proposed control strategy to control the nanopositioning platform.

3.1 Traditional Control Strategy

The traditional single-loop feedback scheme is shown in Fig. 4. In traditional tracking, nanopositioning tracking is achieved through the use of single-loop feedback. The tracking controller commonly used in this scheme is either a first-order integral (I), or a proportional integral (PI). Figure 4 also illustrates the method by which the tracking (Ct_1) and damping controllers (C_d) are combined and used together. This traditional approach can improve the positioning accuracy of the nanopositioning platform to some extent. However, feedback control law is limited in compensating for hysteresis. Due to stability issues, second-order controller in a single-loop is not directly applicable.
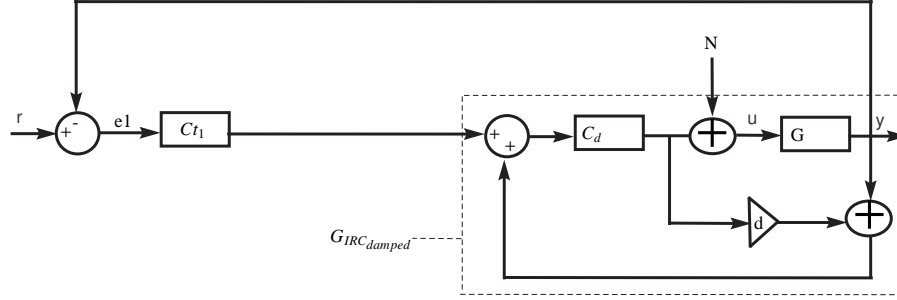
6

Fig. 4. Schematic of the traditional damping+tracking control scheme

3.2 Proposed Control Strategy

An attempt to apply second-order integral tracking to the nanopositioning platform has been proposed that will not affect the stability of the platform. In order to draw a comparison with a single-loop feedback controller, the multi-loop feedback control system is described by the scheme shown in Fig. 5. The overall control algorithm in Fig. 5 consists of two controllers for tracking: the outer-loop feedback uses a first-order integral tracking (Ct_1) with a transfer function of $\{\frac{K_{T2}(s)}{s}\}$, and the inner-loop feedback uses a first-order integral tracking (Ct_2) with a transfer function of $\{\frac{K_{T1}(s)}{s}\}$. The damped system ($G_{IRC_{damped}}(s)$) using the IRC controller has the following transfer function [2]:

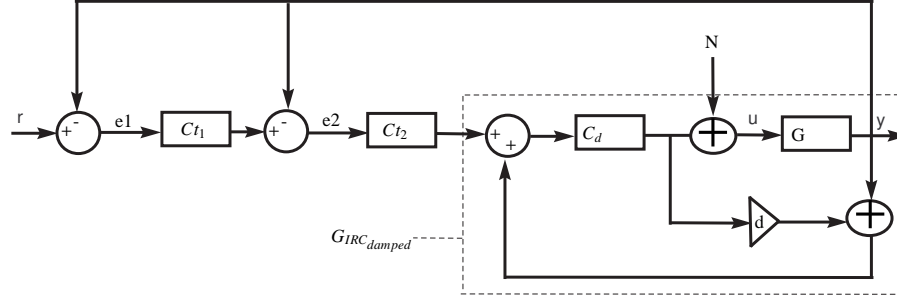$$G_{IRC_{damped}} = \frac{K_d * G}{1 - K_d * (G + d)} \tag{8}$$

Fig. 5. Schematic of the proposed control scheme with dual-loop tracking+damping

The overall transfer function for the multi-loop scheme is given by:

$$\frac{Y(s)}{R(s)} = \frac{K_{T2}K_{T1}k_dG}{K_{T2}K_{T1}k_dG + 1 - dk_d - Gk_d + K_{T1}k_dG} \tag{9}$$

The transfer functions for $K_{T1}(s)$, $K_{T2}(s)$ and $K_d(s)$ are listed in (10):

$$\begin{cases} K_{T1}(s) = \frac{K_{T1}}{s} \\ K_{T2}(s) = \frac{K_{T2}}{s} \\ K_d(s) = \frac{K_d}{s} \end{cases} \tag{10}$$

The characteristics equation for the proposed multi-loop feedback scheme is specified by:

$$s^5 + (2\zeta\omega_p - dK_d)s^4 + (\omega_p^2 - 2\zeta\omega_p dk_d)s^3 +$$
$$(-dK_d\omega_p^2 - K_d\sigma^2)s^2 + K_{T1}K_d\sigma^2 s + K_{T2}K_{T1}K_d\sigma^2 = 0 \tag{11}$$

The transfer function of the normalised fifth-order Butterworth filter is given by:

$$\frac{1}{s^5 + 3.236s^4 + 5.236s^3 + 5.236s^2 + 3.236s + 1} \tag{12}$$

Equation (12) can be rewritten for any given frequency by substituting s with $\frac{s}{\omega_c}$ and this is given by:

$$\frac{\omega_c^5}{\frac{s^5}{\omega_c^5} + 3.236\frac{s^4}{\omega_c^4} + 5.236\frac{s^3}{\omega_c^3} + 5.236\frac{s^2}{\omega_c^2} + 3.236\frac{s}{\omega_c} + 1} \tag{13}$$

The characteristics equation for the Butterworth filter at any given frequency is specified by:

$$s^5 + 3.236\omega_c s^4 + 5.236\omega_c^2 s^3 + 5.236\omega_c^3 s^2 + 3.236\omega_c^4 s +$$
$$\omega_c^5 \tag{14}$$

In order to emulate the Butterworth pattern, the characteristics equation for the multi-loop control strategy must be equated to the characteristics equation for the Butterworth filter; this will determine the values for the feed-through term, damping gain and tracking gains. Thus, (11) must be similar to (14). The following quantities are obtained as a result of linking the two characteristics equations:

$$\begin{cases} 2\zeta\omega_p - dK_d = 3.236\omega_c \\ \omega_p^2 - 2\zeta\omega_p dk_d = 5.236\omega_c^2 \\ -dK_d\omega_p^2 - K_d\sigma^2 = 5.236\omega_c^3 \\ K_{T1}K_d\sigma^2 = 3.236\omega_c^4 \\ K_{T2}K_{T1}K_d\sigma^2 = \omega_c^5 \end{cases} \tag{15}$$

Substituting the above quantities, the value of ω_c can be estimated by solving the following equation using the quadratics polynomial formula:

$$\omega_c^2 - 1.23605806\zeta\omega_p\omega_c + (\frac{\omega_p^2(4\zeta^2 - 1)}{5.236}) \tag{16}$$

The value of the damping gain can be evaluated using the following formula:

$$k_d = \frac{3.236 * \omega_c * \omega_p^2 - 2 * \zeta * \omega_p^3 - 5.236 * \omega_c^3}{\sigma^2} \tag{17}$$

The value of the feed-through term can be calculated using the following equation:

$$d = \frac{2 * \zeta * \omega_p - 3.236 * \omega_c}{k_d} \tag{18}$$

The tracking gains can be valued as follows:

$$k_{T1} = \frac{3.236 * \omega_c^4}{k_d * \sigma^2}, \ K_{T2} = \frac{\omega_c^5}{k_{T1} * k_d * \sigma^2} \tag{19}$$

Using (5), (16) can now be solved and the damped natural frequency ω_c can be determined as $7.7527 * 10^3$ Hz. Having calculated the damped natural frequency, all other variables can now be determined. Table 1 shows the values of the proposed scheme parameters required to achieve the Butterworth pattern.

Table 1. Controller parameters for the simultaneous damping and tracking strategy

Parameter	Value
d	-2.4746
k_d	9770.2
k_{T1}	2521.1
k_{T2}	2395.8

Further analysis to test the tracking performance of the proposed control strategy has been conducted, as will be clear in the following sections.

4 Simulation Results

In this section, the results are presented related to both the frequency and time domains, and error analysis is also conducted. Robustness of the proposed control strategy is also tested in this section.

4.1 Closed-loop Positioning Performance

The simulated frequency response of the proposed multi-loop technique is presented in Fig. 6 and it can be seen that the Butterworth-based filter pattern has been obtained. The pattern is achieved as a result of the tuning method used in Table 1 based on the fifth-order Butterworth filter. The gain margin GM=6.4 dB and phase margin PM=600° are

of optimal values for a robust stable system. An encouraging frequency response has been achieved with regards to better tracking performance as no ripple is exhibited in the passband or stopband and the closed-loop Butterworth-based bandwidth is observed at 1230 Hz. This bandwidth is of a sufficient level to cover the major harmonics that form the triangle wave, resulting in accurate tracking performance and reduced sensitivity to sensor noise.
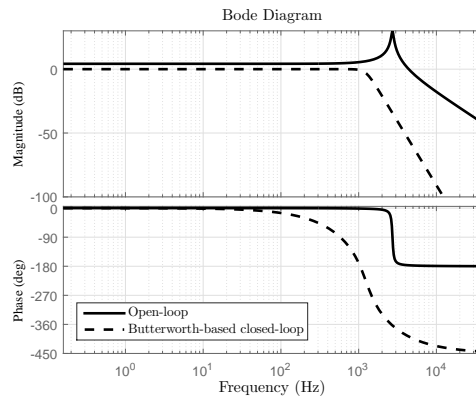

Fig. 6. Open-loop and closed-loop frequency response of the proposed multi-loop control strategy

Bandwidth in nanopositioning is defined as the point at which the closed-loop magnitude response of a given system is exhibiting (at any given point in the passband) a 0 dB gain, and this should not increase or decrease by ±1 dB [7]. The Butterworth-based magnitude response in Fig. 6 does not exceed 0 dB at any passband point; therefore, this is a useful characteristic in achieving accurate tracking performance of the nanopositioning platform.

The root locus has been investigated; it is shown that the poles of the system are at a significant distance from the imaginary axis. The Butterworth pattern is achieved as the tracking gain reaches its design value where the pole at origin with a 0° angle will be shifted further to the left of the imaginary axis. At this point, the distribution of the poles of the fifth-order Butterworth is achieved and the angles of the poles are 0°, ±36° and ±72°.

It is noted that stability is a critical concern when applying, for example, a double-integral tracking controller; applying a second-order integral without the use of the multi-loop feedback scheme causes instability. Hence, the proposed method preserves stability while applying two first-order integral controllers to avoid phase profile. It could be argued that adding another integrator would affect the bandwidth and increase the order of the system unnecessarily however, due to highly nonlinear hysteresis and sensitivity to noise, double integration is warranted. There are two common types of tuning method that provide compensation procedures, either to widen the bandwidth or reduce tracking error; this has been satisfied in this work. For the reasons given above, the multi-loop feedback controller scheme is therefore preferred.

In order to demonstrate the effectiveness of the proposed multi-path feedback controller, a 30 and 40 Hz triangles have been chosen to be tracked with a 20 μm peak, and

simulations performed in MATLAB Simulink. Results for the open- and closed-loop are presented in Fig. 7 (a, b). It can be seen that in the open-loop the tracked signal deviates from the linear because of the presence of hysteresis. As is also clear from Fig. 7(a, b), in the open-loop the tracked signal is experiencing oscillatory behaviour because no damping controller is used. Neither resonance nor hysteretic behaviour is observed in the linear part of the tracked signal, as is shown in Fig. 7 (a, b). The error plot is drawn to illustrate the linear part of the tracked signal, as is shown below. The error signal is directly proportional to the frequency of the tracked signal in a trade-off relationship. Therefore, as the frequency increases, there is a reduction in the linear part, which is an undesirable characteristics. Tracking of the high frequency signal is preferable in nanopositioning due to high speed scanning.
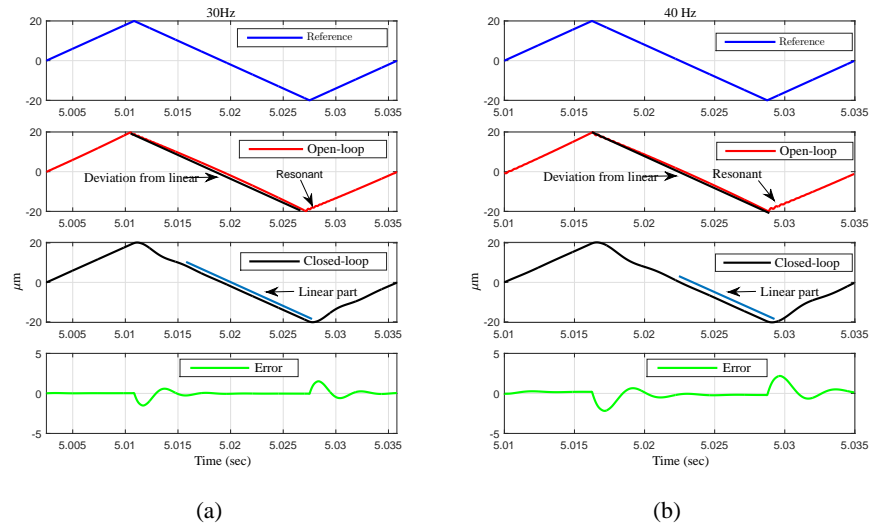

(a)

(b)

Fig. 7. The tracking performance of the platform for a triangle signal in the open- and closed-loop: a- 30; Hz b- 40 Hz

For the proposed dual-loop control strategy depicted in Fig. 4 (b), the error is derived as in the following transfer function:

$$E_1(s) = \frac{R(s)(1 - dk_d(s) - G(s)k_d(s) + K_{T1}(s)k_d(s)G(s))}{1 - dk_d(s) - G(s)k_d(s) + K_{T1}(s)k_d(s)G(s) + K_{T2}(s)K_{T1}(s)K_d(s)G(s)} \quad (20)$$

For the system under consideration, the multi-loop control strategy is type 1; in order to ensure that the steady-state error is acceptable, steady-state error analysis is proposed. For the proposed system, the Butterworth-based controller design is considered; R(s) is

for a ramp and the transfer functions are given by:

$$
\left\{
\begin{array}{c}
R(s) = \frac{1}{s^2} \\[2ex]
K_d(s) = \frac{kd}{s} \\[2ex]
K_{T1}(s) = \frac{K_{T1}}{s} \\[2ex]
K_{T2}(s) = \frac{K_{T2}}{s} \\[2ex]
G(s) = \frac{\sigma^2}{s^2 + 2\zeta\omega_p s + \omega_p^2} \\[2ex]
d
\end{array}
\right\}
\tag{21}
$$

In order to find the steady-state error, the final value theorem is applied as in (22):

$$
e(\infty) = \lim_{s \to 0} sE(s)
\tag{22}
$$

For any given second-order system, the steady-state error to track a ramp using the multi-loop scheme is given by:

$$
e_{1(steady-state)} = \frac{-\sigma^2 + \sigma^2 K_{T1} - d\omega_p^2}{-\sigma^2 + \sigma^2 K_{T1} + K_{T2}K_{T1}\sigma^2}
\tag{23}
$$

Equation (23) can be minimised as in (24) below:

$$
e_{1(steady-state)} = \frac{-d\omega_p^2}{K_{T2}K_{T1}\sigma^2} \equiv \frac{d\omega_p^2}{K_{T2}K_{T1}\sigma^2}
\tag{24}
$$

In order to achieve accurate tracking, $\forall G(s)|_{s=0} = 1$, it is assumed $\sigma^2 = w_p^2$ and then (24) can be approximated as in the equation below:

$$
e_{1(steady-state)} = \frac{d}{K_{T2}K_{T1}}
\tag{25}
$$

In solving (25), zero steady-state error is almost achieved. For the system under consideration, after substantiating the quantities as in Table 1 and when the values of $\sigma^2 = 4.746 * 10^8$ and $\omega_n^2 = 2.927 * 10^8$ are known, the error at steady-state can now be estimated as e(∞)=0.041735.

In nanopositioning, the raster scan trajectory is achieved by applying triangle wave in the x-axis and a ramp in the y-axis. The transient error occurs at the turn-around area of the triangular waveform at the end of each scan line, thereby promoting scanning speed (frequency) and amplitude of the driven signal. The error at the turn-around is relatively large due to the high frequency components of the triangle wave and hysteresis nonlinearity. The appearance of the transient error is due to system behaviour when encountering disturbance on attempting to track the triangle wave. The transient error

can, however, be reduced by increasing the gain of the controller. Due to the fact that the controller design is simultaneously tuned for damping and tracking gains, changing the gain to reduce the transient error is difficult. Although the transient error at the turn-around adds some distortion to the raster scan image, its effect on the raster scan is limited because only the linear part is taken into account.

In order to demonstrate the strength and effectiveness of the proposed control strategy, a comparative error analysis of the multi-loop and single-loop feedback schemes, presented in [9], is examined in the following part.

In a single-loop feedback controller, the controller takes the tracking error (r(t)-y(t)) as input; this is called output feedback. In this case, the calculation of the control signal is based on the plant output and is subject to large control actions when the set-point undergoes a sudden change. On the other hand, in the multi-loop feedback control, the controller takes the error as input where the outer-loop defines the set point for the inner-loop; this is called error feedback.

Tracking a triangle wave (high frequency components) in nanopositioning generates significant positioning error at high frequencies, and the effect of hysteresis is also significantly more common at high frequencies. The RMS error plot is plotted across various frequency changes, as is clear in Fig. 8.
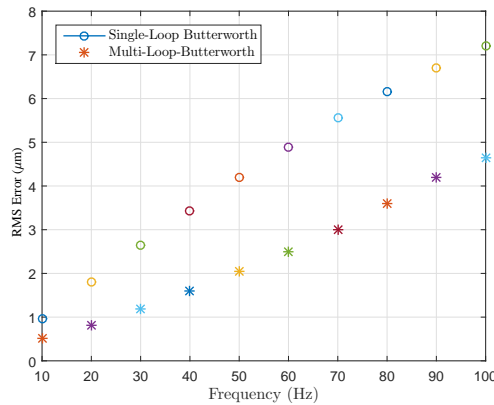

Fig. 8. A comparison of RMS error across various frequency changes

The positioning error is substantially improved by using the multi-loop feedback scheme in the presence of hysteresis; thus the use of this scheme in nanopositioning applications is preferred. To conclude, the performance of the multi-loop feedback scheme is better than that of the single-loop feedback scheme.

Further analysis to test the robustness of the proposed control strategy has been conducted, as will be clear in the following section.

4.2 Robustness to Resonance Frequency Variation and Disturbance Rejection Profiles

Robustness refers to the ability of the closed-loop system to be insensitive to parameter variation. Disturbance rejection is another important performance index in nanoposi-

tioning applications that needs to be evaluated. This refers to the ability of a system to be insensitive to exogenous disturbances. In this section, both robustness to resonance frequency changes and the disturbance rejection profiles at these changed resonance frequencies are evaluated. Developing an accurate dynamic model in a positioning system is a difficult task because of the complex mechanical structure of the nanopositioning stage. In order to account for these uncertainties, designing a control algorithm capable of dealing with uncertainties is essential [4, 5].

In order to test the capability of the proposed scheme to accommodate resonant frequency variation, a 5% and 10% reduction in the resonant frequency is considered. Resonance frequency changes can occur due to loading of the nanopositioners with different samples. The open-loop and closed-loop frequency response for all these changes is plotted in Fig. 9 (a).
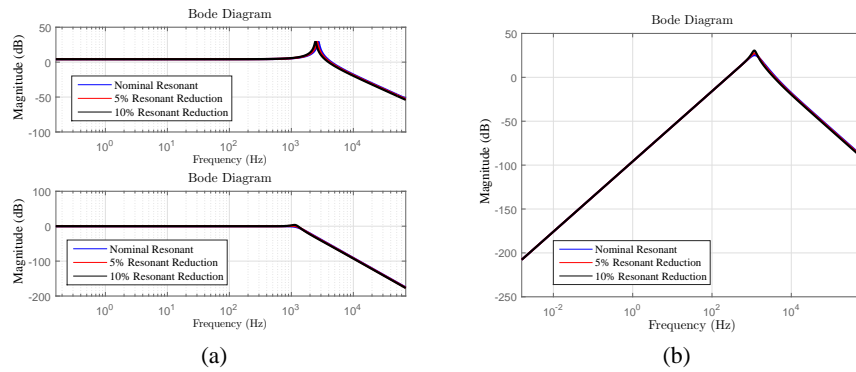

(a)   (b)

Fig. 9. a- Open-loop and closed-loop magnitude response for resonant frequency changes b- Disturbance rejection across various resonant frequency changes

The sensitivity of the proposed method is reflected in Fig. 9 (a). It can be seen that a 5% or 10% reduction in resonance frequency does not have a significant influence on the closed-loop; therefore, the proposed control scheme is robust to resonance frequency changes.

The disturbance rejection transfer function for the proposed system is given by:

$$\frac{Y(s)}{N(s)} = \frac{G(s)(1 - K_d(s)d)}{1 - K_d(s)d + G(s)K_d(s) + G(s)K_{T1}(s)K_d(s) + G(s)K_{T2}(s)K_{T2}(s)K_d(s)} \quad (26)$$

In order to test the ability of the controller to attenuate external disturbances, the bode plot for the transfer function in (26) is depicted in Fig. 9 (b). From the figure, it can be seen that changing the resonant frequency by a 5% or 10% reduction does not have a significant influence on the disturbance rejection profile. Significant disturbance rejection is provided at a relatively low frequency up to 1000 Hz; nonetheless, the multi-loop feedback scheme does not exhibit significant disturbance rejection near the resonant frequency. Due to multiple integrals in the multi-loop feedback controller scheme, the steady-estate error is almost zero.

5 Conclusion

In this paper, a hybrid damping and tracking strategy with dual-loop tracking is proposed and its performance tested via simulation. The developed control strategy emulates the Butterworth pattern for maximally flat in-bandwidth response. Simulation results confirm the effectiveness of the proposed method in terms of high tracking accuracy in the presence of hysteresis and robust stability in the presence of resonance frequency changes.

References

1. Aphale, S.S., Bhikkaji, B., Moheimani, S.R.: Minimizing scanning errors in piezoelectric stack-actuated nanopositioning platforms. IEEE Transactions on Nanotechnology 7(1), 79–90 (2008)
2. Aphale, S.S., Fleming, A.J., Moheimani, S.R.: Integral resonant control of collocated smart structures. Smart Materials and Structures 16(2), 439 (2007)
3. Bouc, R.: Forced vibration of mechanical systems with hysteresis. In: Proceedings of the fourth conference on non-linear oscillation, Prague, Czechoslovakia (1967)
4. Dong, J., Salapaka, S.M., Ferreira, P.M.: Robust control of a parallel-kinematic nanopositioner. Journal of dynamic systems, measurement, and control 130(4), 041007–041007–15 (2008), http://dx.doi.org/10.1115/1.2936861
5. Eielsen, A.A., Vagia, M., Gravdahl, J.T., Pettersen, K.Y.: Damping and tracking control schemes for nanopositioning. IEEE/ASME Transactions on Mechatronics 19(2), 432–444 (2014)
6. Jain, S., Garg, M., Swarup, A.: Disturbance rejection of nanopositioner using internal model control. i-Manager's Journal on Electronics Engineering 2(4), 1–7 (2012)
7. Namavar, M., Fleming, A.J., Aleyaasin, M., Nakkeeran, K., Aphale, S.S.: An analytical approach to integral resonant control of second-order systems. Mechatronics, IEEE/ASME Transactions on 19(2), 651–659 (2014)
8. Russell, D., Fleming, A.J., Aphale, S.S.: Simultaneous optimization of damping and tracking controller parameters via selective pole placement for enhanced positioning bandwidth of nanopositioners. Journal of Dynamic Systems, Measurement, and Control 137(10), 101004–101004–8 (2015), http://dx.doi.org/10.1115/1.4030723
9. Russell, D., San-Millan, A., Feliu, V., Aphale, S.S.: Butterworth pattern-based simultaneous damping and tracking controller designs for nanopositioning systems. Frontiers in Mechanical Engineering 2, 2 (2016), http://journal.frontiersin.org/article/10.3389/fmech.2016.00002
10. Teo, Y.R., Russell, D., Aphale, S.S., Fleming, A.J.: Optimal integral force feedback and structured pi tracking control: Application for high speed confocal microscopy. IFAC Proceedings Volumes 47(3), 11793–11799 (2014)
11. Wen, Y.K.: Method for random vibration of hysteretic systems. Journal of the engineering mechanics division 102(2), 249–263 (1976)
12. Xu, Q., Tan, K.K.: Advanced Control of Piezoelectic Micro-/nano-positioning Systems. Springer (2015)
13. Yong, Y.K., Bazaei, A., Moheimani, S.O.R.: Control of a high-speed nanopositioner for lissajous-scan video-rate afm. In: Control Conference (AUCC), 2013 3rd Australian. pp. 171–176 (2013)
14. Zhou, J., Wen, C.: Adaptive backstepping control of uncertain systems: nonsmooth nonlinearities, interactions or time-variations. Springer (2008)